A Convex Selective Segmentation Model based on a Piece-wise Constant Metric Guided Edge Detector Function

Muhammad Shahkar Khan
University of Peshawar
Haider Ali
University of Peshawar
Muhammad Zakarya (mohd.zakarya@awkum.edu.pk)
Abdul Wali Khan University Mardan https://orcid.org/0000-0001-7070-6699
Santosh Tirunagari
Middlesex University London
Ayaz Ali Khan
University of Lakki Marwat
Rahim Khan
Abdul Wali Khan University Mardan
Aftab Ahmed
Abdul Wali Khan University Mardan
Lavdie Rada
Bahcesehir University: Bahcesehir Universitesi

Research Article

Keywords:

Posted Date: December 30th, 2022

DOI: https://doi.org/10.21203/rs.3.rs-2391118/v1

A Convex Selective Segmentation Model based on a Piece-wise Constant Metric Guided Edge Detector Function

Muhammad Shahkar Khan[1], Haider Ali[1], Muhammad Zakarya[2,3,+,*], Santosh Tirunagari[4,+], Ayaz Ali Khan[5,+], Rahim Khan[2], Aftab Ahmed[2], and Lavdie Rada[6]

[1]Department of Mathematics, University of Peshawar, Pakistan
[2]Department of Computer Science, Abdul Wali Khan University, Mardan, Pakistan
[3]Faculty of Computing and IT (FCIT), Sohar University, Sultanate of Oman
[4]Middlesex University, London, UK
[5]Department of Computer Science, University of Lakki Marwat, Khyber Pakhtunkhwa, Pakistan
[6]Biomedical Engineering Department, Bahcesehir University, Besiktas, Istanbul, Turkey
[*]mohd.zakarya@awkum.edu.pk
[+]these authors contributed equally to this work

ABSTRACT

The challenge of segmentation for noisy images, especially those that have light in their backgrounds, is still exists in many advanced state-of-the-art segmentation models. Furthermore, it is significantly difficult to segment such images. In this article, we provide a novel variational model for the simultaneous restoration and segmentation of noisy images that have intensity inhomogeneity and high contrast background illumination and light. The suggested concept combines the multi-phase segmentation technology with the statistical approach in terms of local region knowledge and details of circular regions that are, in fact, centered at every pixel to enable in-homogeneous image restoration. The suggested model is expressed as a fuzzy set and is resolved using the multiplier alternating direction minimization approach. Through several tests and numerical simulations with plausible assumptions, we have evaluated the accuracy and resilience of the proposed approach over various kinds of real and synthesized images in the existence of intensity inhomogeneity and light in the background. Additionally, the findings are contrasted with those from cutting-edge two-phase and multi-phase methods, proving the superiority of our proposed approach for images with noise, background light, and inhomogeneity.

1 Introduction

Image segmentation is an approach of partitioning a particular image into several small regions which share certain known characteristics, leading to meaningful and easy post-processing analyzes. Many industries, including medical imaging, object identification and recognition, traffic control systems, etc., use image segmentation in many practical ways. The wide range of application in image processing leads to significantly different segmentation techniques with respect to the same specific object/region labeling characteristic. Segmentation of all the objects in a scene was the first image segmentation task. Such a task was firstly processed with simple methods, such as thresholding method, region growing, etc., further followed by sophisticated techniques, in particular, artificial intelligence, such as variational models or constitutional neuron network based models.

Variational segmentation models, leading to partial differential equations, are one of the well known segmentation techniques due to their robustness, computational advantage, and a well settled mathematical background. The two main classes of variational models are: (i) region based models[1]; and (ii) edge based models[2–4]. Region based models use statistical characteristic of the region to be segmented whereas edge based techniques get advantages of the geometrical properties of the first and second derivative. One of the most important region based image segmentation models, extensively studied in the last twenty years, is the Mumford-Shah (MS) model[1]. The energy minimization of the MS model aims to approximate the true solution by an optimal piece-wise smooth approximations. Even though, the MS minimization model is non-

convex and very challenging. On the other hand, the edge based methods in comparison with region based methods have, as reported in previous studies[12,39,44], the main drawback which is the lack of robustness in dealing with noisy images. To get the benefits of both region and edge based valuable properties, leading to better segmentation accuracy and robustness, mixed models have been introduced in the literature[5–7]. This combination uses the region information globally, whereas, the image gradient information are used locally for edge identification.

As an alternative to variational models different techniques have been proposed over years such as multi-atlas segmentation projected and shown to be useful[8,9] for images with well known preliminary data, non-parametric statistical segmentation[10–12] to handle texture segmentation, wavelet method[13], etc. For more segmentation methods reader is referred to[14–22] and the references therein. In the wide variety of segmentation methods supervised segmentation techniques have been broadly investigated in machine learning and pattern recognition[23–27]. However, the large training sets makes them limited by the lack of generalization to previously unseen object classes.

In the last decade, in many applications, like object tracking, medical treatment, surgery, traffic control systems, etc., only one object (or a few objects) of interest are aimed to be extracted. For such problems, selective/ interactive image segmentation models are more useful. Selective object selection enables users to select objects of interest through interactively providing inputs such as markers, strokes, bounding boxes, etc. In the last years many algorithms were proposed to solve this problem varying from graph cut optimization energy[28–30], convex relaxation methods[31,32], weighted geodesic distances[33], edge-based method[5,34,35], random walks[36], fuzzy membership function[37–39], etc. In the last years, the variational models which combine region and edge information show successful selective segmentation results.

By applying a set of marker points on the contour of importance region of interest, the authors in[34] were the first to provide geometrical limitations to the geodesic active contour selective segmentation model. The authors in[?] improved the robustness of the results, particularly in regions with noise, by combining the geometrical limitations provided by[?] with region-based terms. A geometrical constraint and adaptive local band technique that takes into consideration the intricate elements of a picture was suggested by[40]. Similarly, the authors in[35] proposed a dual level set variational model, which uses two-level set functions to separate the aimed object from the rest of all meaningful objects. The first level set is used for segmentation of all edges of the objects in the given image whereas the other one is used to select the object that is near to the geometry constraints. Furthermore,[41] proposed a region based model which takes into account multiple features and appearance context information with application in 3D liver segmentation.[42] utilized image channels average and proposed a selective segmentation model which can extract in-homogeneous and textural objects. Recently, the work presented in[43] included weight function into the MS model and proposed a second-order convex model for image segmentation, in particular, selective segmentation. Even though, the above-mentioned methods show good numerical performance there are still some challenging images demonstrating their fail[44,45].

In this paper, we propose a new two-stage weighted convex selective image segmentation model which combines edge detector function guided by a metric function into a second-order convex model for segmentation, in particular, selective segmentation. In the first stage, an edge detector function will detect the edges of interest and ignore unnecessary edges, whereas the second step deal with a weight function obtained based on novel edge detector function. Alternating direction method has been used as an appropriate numerical algorithm and uniqueness and existence of the minimizer of the suggested model for image segmentation has been shown. Following are the major contributions of our work.

- It is proposed to combine an edge detector function directed by a metric function with a convex second-order segmentation model to create a bi-phase weighted convex selective image segmentation model.
- In the presence of high contrast light in the background, a variational model for the combined restoration and segmentation of noisy images with intensity inhomogeneity is given.
- The suggested model is expressed as a fuzzy set and is resolved using the multiplier alternating direction minimization approach.

The remainder of this article is structured as follows. Section 2 provides a quick overview of the relevant segmentation models. The variational formulation of our models for tasks requiring selective segmentation is described in Section 3. The numerical algorithm and convergence analysis of the model are described in Section 4. In Section 5, numerical experiments demonstrating the effectiveness of our strategy are provided.

In this part, we demonstrate how, when compared to previous selective segmentation strategies, the suggested strategy streamlines user interactions to a few clicks and produces relatively decent results. Section 6 provides a discussion and recommendations for the future to wrap up our effort.

2 Related Work

In this section, we divide the related work into tow different types: (i) variational segmentation models; and (ii) selective segmentation models.

2.1 Variational Segmentation Models

Since the original Mumford and Shah functional is non-convex and in practice difficult to find smooth approximations to solve the minimization problem several approximations have been proposed. One of the most important approximations is the level set approximation proposed by Chan-Vese (CV)[46]. The level set function introduced by Osher-Sethian[47] was used in the CV model as a way to allow topological changes for the curve evolution of the Lipschitz continuous level set function (LSF). Chan-Vese first work[46] assumes that the given image consists of foreground and background which can be represented as piece-wise constant function. Afterwards, this model was extended to multiphase segmentation[48] and further modified into many other ideas[49–51]. Lastly,[52] proposed a new variation of the MS model. The model blends the idea of image restoration[53] and image segmentation into a two-stage convex segmentation model. Due to convexity, Split-Bregman algorithm[54,55] has been used as a solver and a unique smooth minimizer has been found. Using a thresholding procedure the image segmentation is achieved. The threshold for the segmentation is chosen automatically using clustering methods. In the following, we shortly give the minimization function for the MS model[1] and further summarize[52] model.

The main objective function of the MS model[1] lead to the solution of the following minimization problem:

$$\inf_{z,\Gamma}\left\{\frac{\alpha}{2}\int_{\Omega}|z(\mathbf{x})-f(\mathbf{x})|^2d\mathbf{x}+\frac{\beta}{2}\int_{\Omega\setminus\Gamma}|\nabla z(\mathbf{x})|^2d\mathbf{x}+\mathscr{H}^1(\Gamma)\right\}$$

where $\Omega\subset R^2$ is a connected bounded open set with Lipschitz boundary, Γ a compact curve in Ω, $f:\Omega\longrightarrow R$ be a given image, $z(\mathbf{x}):\Omega\longrightarrow R$ a piece-wise smooth function representing the given image $f(\mathbf{x})$, $\mathscr{H}^1(\Gamma)$ represents the one dimensional Hausdorff measure computing the length of Γ for a fixed curve, α,β are positive constants.

Based on the MS model idea,[52] proposed a variational image segmentation model composed of two stages. In the first stage, the given image is estimated with a smooth function by solving the following convex minimization problem:

$$\min_{z(\mathbf{x})\in W^{1,2}(\Omega)}\Big[\int_{\Omega}|\nabla z(\mathbf{x})|d\mathbf{x}+\frac{\alpha}{2}\int_{\Omega}|\nabla z(\mathbf{x})|^2d\mathbf{x}+\frac{\beta}{2}\int_{\Omega}|z(\mathbf{x})-f(\mathbf{x})|^2d\mathbf{x}\Big],\tag{1}$$

where $W^{1,2}(\Omega)=\left\{v\in L^2(\Omega)/\partial_j v\in L^2(\Omega),j=1,2\right\}$ is a Banach space with

$$L^2(\Omega)=\left\{f(\mathbf{x})/\left(\int_{\Omega}f^2(\mathbf{x})d\mathbf{x}\right)^{1/2}<\infty\right\},$$

and α,β are positive constants. Once $z(\mathbf{x})$ is computed, segmentation is carried out through the second stage thresholding the obtained $z(\mathbf{x})$. The threshold can be provided interactively by the uses or obtained automatically by any clustering method, such as convex K-means or K-means methods[56,57].

2.2 Selective Segmentation Models

In terms of selective image segmentation task an object of interest is aimed to be segmented from the given image. Let us suppose that the object of interest is placed inside M given points $A=\left\{\mathbf{x_1^*},\mathbf{x_2^*},...,\mathbf{x_M^*}\right\}$. A distance function $d(\mathbf{x}):\Omega\longrightarrow R$ can be defined as[5]

$$d(\mathbf{x})=\prod_{j=1}^{M}\left\{(1-\exp^{\left(\frac{-|\mathbf{x}-\mathbf{x_j^*}|^2}{2\tau^2}\right)}\right\},\quad\forall\mathbf{x}\in\Omega\tag{2}$$

where $\tau > 0$ is a constant. We clearly notice that the distance function is near to zero at the neighborhood of the marker points and increases if the point is far away from the marks. This property is same for other distance function formulation found in literature[5].

On the other hand, the information of edges in a given image can be detected through the properties of the first variation of the function with the supposition that the function is piece-wise smooth. Such a edge detection function can be defined as follows:

$$g(\mathbf{x}) = \frac{1}{1+\beta|\nabla f(\mathbf{x})|^2}. \tag{3}$$

From the formulation, we can easily see that the $g(\mathbf{x})$ has an almost zero vales near edges and a value of one on the smooth regions of the foreground or the background. Considering the properties of this two functions[34] proposed the following minimization functional as a solution for the selective segmentation problem:

$$\min_{\Gamma} \int_{\Gamma} d(\mathbf{x})g(\mathbf{x})ds,$$

where $d(\mathbf{x})$ is a distance function and $g(\mathbf{x})$ is edge detection function. The combination aims to stop in local minima guided by the edge function. As the model has difficulties for noisy images,[5] introduced intensity fitting terms similar to Chan-Vese model[46] and improved the[34] model in the following formulation:

$$\min_{\Gamma,c_1,c_2} \Big[\mu \int_{\Gamma} d(\mathbf{x})g(\mathbf{x})ds + \lambda_1 \int_{\Omega in} |f(\mathbf{x}) - c_1|^2 dxdy + \lambda_2 \int_{\Omega out} |f(\mathbf{x}) - c_2|^2 dxdy\Big], \tag{4}$$

where λ_1, λ_2 and μ are constant used to adjust the balance between regularity and fidelity terms. The boundary between Ωin and Ωout is Γ, constants c_1 and c_2 are to be optimized. Using the level set formulation of the above equation and minimizing respect to the unknowns lead to an Euler-Lagrange equation which can be solved with different solvers and techniques. In the continuation of those methods, new ideas were introduced such as adaptive local band level set method by[40], continuous-domain convex active contour model by Nguyen[58], weighted variational model by[59] for selective segmentation with application to medical images, etc. The[59] model gets its motivation by[52] model combining with a weight function as follows:

$$\min_{u(x)\in W^{1,2}(\Omega)} \Big[E(z(\mathbf{x})) := \int_{\Omega} |\nabla z(\mathbf{x})| d\mathbf{x} + \frac{\alpha}{2}\int_{\Omega} |\nabla z(\mathbf{x})|^2 d\mathbf{x} + \frac{\beta}{2}\int_{\Omega} \omega^2 |z(\mathbf{x}) - f(\mathbf{x})|^2 d\mathbf{x}\Big], \tag{5}$$

where ω is a weight function to adjust the fidelity and smoothing terms and is defined as:

$$\omega^2(\mathbf{x}) = 1 - d(\mathbf{x})g(\mathbf{x}), \tag{6}$$

with $\omega(\mathbf{x}) \in (0, 1]$. Similar to work presented in[52], the two-stages strategy has been used. In the first stage, a smooth approximation of the input image is obtained by hiring a weighted function which provides a larger value for the target region and smaller values for other regions. In the second stage, they make use of the obtained approximation to perform a thresholding procedure and obtain the object of interest.

3 The Proposed Model

We describe our novel model and its mathematical analysis in this part. There are two phases in our process. In the first phase, we identify a smooth minimizer by solving a minimization problem based on a specified marker pointing within the object/s of interest. Then, in the second stage, we do segmentation using basic thresholding.

3.1 Description of the Proposed Model

Inspired by the convexity, uniqueness, and existence of the minimizer for[43] model, we took a closer look to the weighted term that is utilized for adjustment of the fidelity and the smoothing terms in the proposed energy function. The edge detector function $g(\mathbf{x})$ is defined all over the image rather than the objects of interest as required in the selective segmentation task.

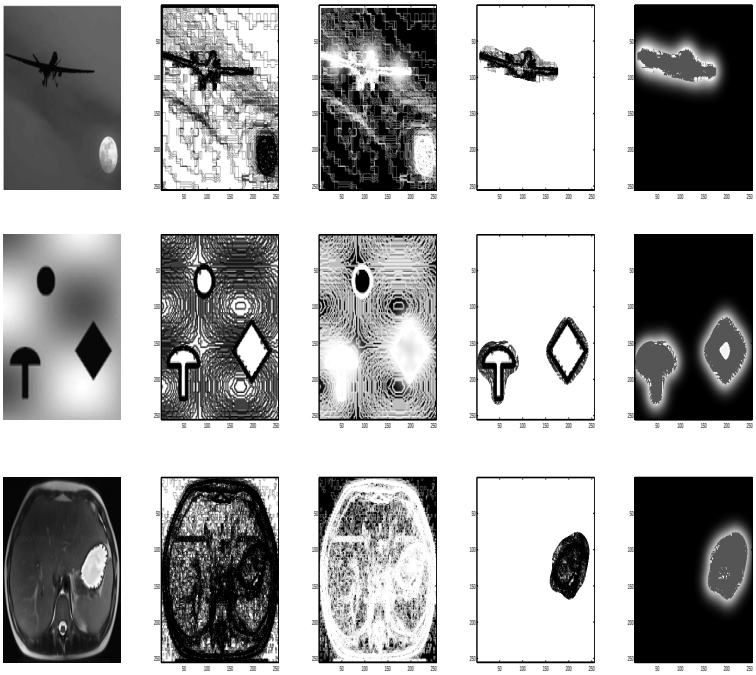

(a) Given image (b) Liu edge function (c) Liu weight function (d) Our edge function (e) Our weight function

Figure 1. Segmenting the Drone image, shapes image, and MRI brain image. Segmented results of[43] and our edge and weighted function

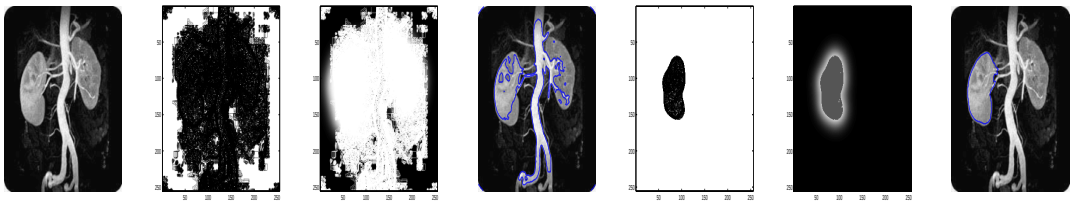

(a) Given image (b) Liu edge function (c) Liu weight function (d) Liu segmentation (e) Our edge function (f) Our weight function (g) Our segmentation

Figure 2. Edge and weight function comparison between[43] and the proposed model for image segmentation of kidney images.

(a) Given image (b) Liu segmentation (c) Our segmentation (d) Liu segmentation (e) Our segmentation

Figure 3. Successful selective segmentation comparison of both Liu and the proposed model for different knee structures with markers placed in each of those structures.

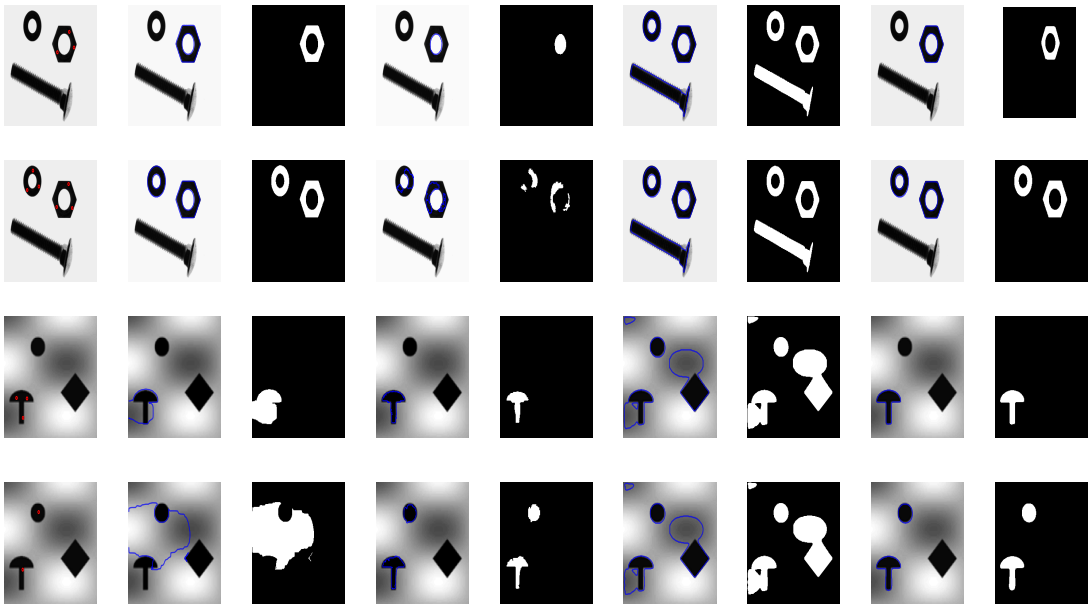

(a) Given image with markers (b) Mabood et al. model (c) Mabood et al. segmented result (d) Rada et al. model (e) Rada et al. segmented result (f) Liu et al. model (g) Liu et al. segmented result (h) Our model (i) Our segmented result

Figure 4. Segmenting of one and multi objects image. Segmented result of[42] model;[35];[43] model, and results of our model.

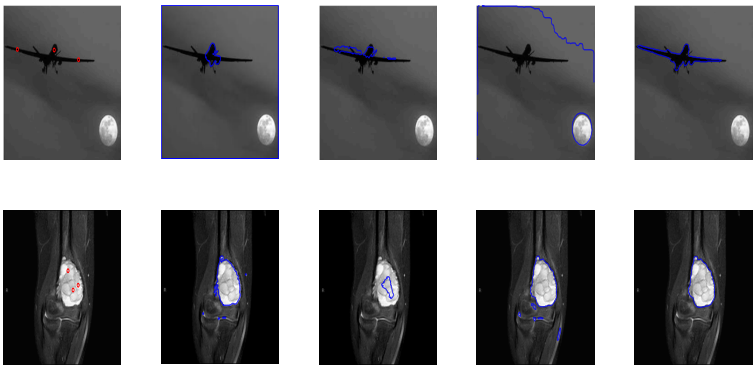

(a) Image with given markers (b) Mabood et al. model (c) Rada et al. model (d) Liu et al. model (e) Our model

Figure 5. Comparison results of[42] model,[35],[43] model and the proposed model for segmentation of MRI Knee image.

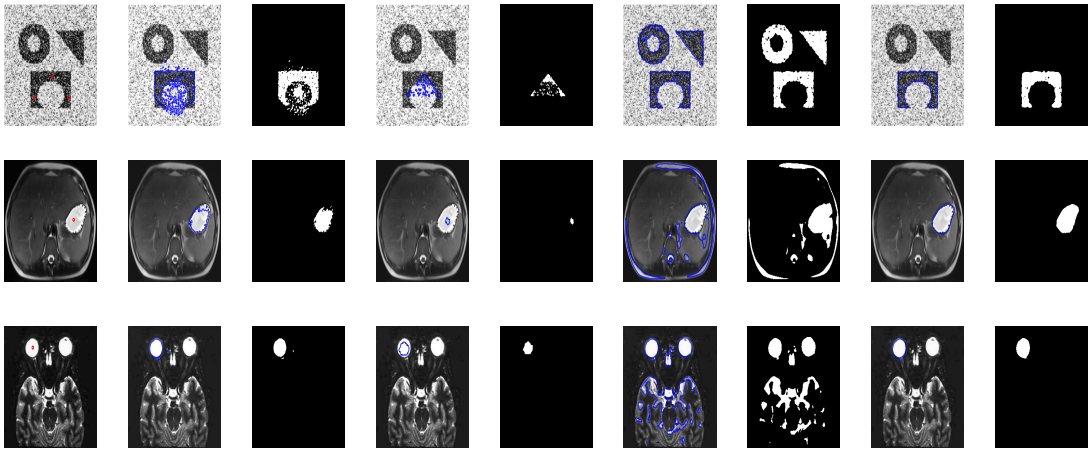

(a) Give image with markers (b) performance of Mabood et al. model (c) Mabood et al. segmented result (d) performance of Rada et al. model (e) Rada et al. segmented result (f) performance of Liu et al. model (g) Liu et al. segmented result (h) performance of Our model (i) Our segmented result

Figure 6. Segmenting the synthetic image in presence of noise in the first row, MRI eye image and cancer image with[42] model,[35],[43] model, and our model.

For a better understanding, we plot this function in Fig. 1 and 2 third column.[43] formulation for the edge function directly influences the weight function $\omega(\mathbf{x})$ which can be witnessed in the third column of Fig. 1 and 2.

To have a function which detects edges of interest given some markers we define the following metric guided edge detector function:

$$g_d(\mathbf{x}) = \begin{cases} 1; & if d(\mathbf{x}) > T \\ g(\mathbf{x}); & if d(\mathbf{x}) < T \end{cases} \tag{7}$$

where T represents the threshold value. Overall this work we choose a threshold value $T = 0.3$. The performance of edge detector function $g_d(\mathbf{x})$ of our model can be seen in Fig. 1 and 2 fifth column. It can be observed that our edge detector function g_d captures only the edges of interest near the given markers. Based on $g_d(\mathbf{x})$, we define the novel weight function i.e. the metric guided weight function $\omega_d(\mathbf{x})$ in the following steps:

$$\omega^2(\mathbf{x}) = 1 - d(\mathbf{x}) g_d(\mathbf{x}), \tag{8}$$

$$\omega_d(x) = \begin{cases} 0.3; & \text{if } \omega^2(x) > T_1 \\ 0.2; & \text{if } T_2 < \omega^2(x) < T_1 \\ 0.1; & \text{if } T_3 < \omega^2(x) > T_2 \\ 0; & \text{if } 0 < \omega^2(x) > T_3 \end{cases} \tag{9}$$

where the threshold values T_1, T_2 and T_3 are chosen as 0.9, 0.6 and 0.3, respectively. The purpose of these threshold values is to assign suitable weights to the objects in a given image and specially to the object of interest. The performance of the novel weight function $\omega_d(\mathbf{x})$ can be observed in the fourth column of Fig. 1 and 2. It can be seen that $\omega_d(\mathbf{x})$ mainly gives weights to the object of interest and tries to ignore other unnecessary objects.

Taking into account the convex model of Cai at al. in equation (1) and the above analysis for the weight function, we propose the following minimization model for the selective segmentation problem:

$$\min_{z \in W^{1,2}(\Omega)} \Big[F(z) := \int_\Omega |\nabla z(\mathbf{x})| d\mathbf{x} + \frac{\alpha}{2} \int_\Omega |\nabla z(\mathbf{x})|^2 d\mathbf{x} + \frac{\beta}{2} \int_\Omega \omega_d |z(\mathbf{x}) - f(\mathbf{x})|^2 d\mathbf{x} \Big]. \tag{10}$$

Here are some comparisons between our model and other selective segmentation models that are currently available. In order to compute numerically, existing selective models must employ level set approaches or membership functions, which might add to the computing burden. In contrast to the suggested model, whose convexity is proved in Appendix 1, references[5,23] indicate sensitivity to the initialization in the tests. The existence and uniqueness of the minimizer can be verified in our model. It is possible to create a large number of reliable and effective numerical algorithms. After obtaining the answer of (10), the segmentation may be obtained in the second step by thresholding.

3.2 Mathematical Analysis

Following equation (1) and[43] we can conclude the following:

Proposition 1: Let $f \in L^2(\Omega)$ and $\inf_{\mathbf{x}\in\Omega} \omega_d(\mathbf{x}) > 0$. Then model (10) is strictly convex and there exists a unique minimizer $z(\mathbf{x}) \in W^{1,2}(\Omega)$.

Proof: From the condition $\inf_{\mathbf{x}\in\Omega} \omega_d(\mathbf{x}) > 0$ and equation (9) $\omega_d(\mathbf{x})$ is bounded. Let $M_1 \leq \omega_d(\mathbf{x}) \leq M_2$, where $M_1, M_2 > 0$.

Chose $z_0 = 0$, we have

$$\begin{aligned} 0 &\leq \inf_{z\in W^{1,2}(\Omega)} F(z) \\ &\leq F(z_0) = \frac{\beta}{2}\int_\Omega \omega_d f^2 dtextbfx \\ &\leq \frac{M_2^2\beta}{2}||f||^2_{L^2(\Omega)} \\ &< +\infty \end{aligned}$$

Thus $\inf_{z\in W^{1,2}(\Omega)} F(z)$ must exist.

We now prove that $F(z)$ is coercive. It is clear that

$$||\nabla z||_{L^2(\Omega)} \leq \sqrt{\frac{2}{\alpha}F(z)} \tag{11}$$

and

$$||z||_{L^2(\Omega)} \leq ||z-f||_{L^2(\Omega)} + ||f||_{L^2(\Omega)}. \tag{12}$$

Furthermore,

$$\begin{aligned} 0 &\leq \frac{M_1^2(\beta)}{2}\int_\Omega |z-f|^2 dxdy \\ &\leq \frac{\beta}{2}\int_\Omega \omega_d |z-f|^2 dxdy \leq F(z), \end{aligned}$$

which yields

$$||z-f||_{L^2(\Omega)} \leq \sqrt{\frac{2}{M_1^2\beta}F(z)}. \tag{13}$$

Combining equation (11), (12) and (13) we have

$$\begin{aligned} ||z||_{W^{1,2}(\Omega)} &\leq ||z-f||_{L^2(\Omega)} + ||\nabla z||_{L^2(\Omega)} \\ &\leq \left(\sqrt{\frac{2}{\alpha}} + \sqrt{\frac{2}{M_1^2\beta}}\right)\sqrt{F(z)} + ||f||_{L^2(\Omega)}, \end{aligned}$$

which demonstrates that $F(z)$ is coercive.

This should be noted that $W^{1,2}(\Omega)$ is a reflective Banach space, and from (10) the $F(z)$ is convex, lower semi continuous, and also coercive. Based on these assumptions, we concluded that the minimizer of $F(z)$ will be located in $W^{1,2}(\Omega)$[52,60].

Finally, this is assured and guaranteed from the strict convexity property of $F(z)$ that the minimizer will be unique.

Proposition 2: Let $f \in L^2(\Omega)$ and $\inf_{\mathbf{x}\in\Omega} \omega_d(\mathbf{x}) > 0$, then the unique minimizer $z^*(\mathbf{x})$ of model (10) meets the inequality $\inf_{\mathbf{x}\in\Omega} f(\mathbf{x}) \leq z^*(\mathbf{x}) \leq \sup_{\mathbf{x}\in\Omega} f(\mathbf{x})$.

Proof: Considering the properness of $F(z)$, as shown in Proposition 1, and with the supposition that z_n be a sequence (minimizing); thus we can find a constant $M > 0$ so that $F(z_n) \leq M$ where $n \in N$. In such a manner, $||\nabla z_n||_{L^2(\Omega)}$ are uniformly bounded. Moreover,

$$\frac{\beta M_1^2}{2}||z_n - f||^2_{L^2(\Omega)} \leq \frac{\beta}{2}\int_\Omega |z_n - f|^2 d\mathbf{x} \leq M,$$

for all $n \in N$.
This yields that $||z_n - f||_{L^2(\Omega)}$ is uniformly bounded and hence

$$||z_n||_{L^2(\Omega)} \leq ||z_n - f||_{L^2(\Omega)} + ||f||_{L^2(\Omega)}$$

is uniformly bounded.

Therefore, as a measure to ∇z^*, ∇z_n converges weakly in $W^{1,2}(\Omega)$, and z_n converges strongly to some z^*. Since $F(z)$ is lower semi-continuous, we have

$$F(\liminf_{n\to\infty} z_n) \leq \liminf_{n\to\infty} F(z_n),$$

which implies that z^* is the unique solution to (10).

Let $\alpha = \inf f$ and $\beta = \sup f$. We remark that $u \to \omega_d|u - f|^2$ is decreasing in $(0, f)$ and increasing in $(f, +\infty)$. Therefore, if $C \geq f$, we have

$$\omega_d|\min(u, C) - f|^2 \leq \omega_d|u - f|^2.$$

Let $C = \beta = \sup f$, we get

$$\int_\Omega \omega_d|\min(z^*, \beta) - f|^2 d\mathbf{x} \leq \int_\Omega \omega_d|z^* - f|^2 d\mathbf{x} \tag{14}$$

Similarly, we can prove that

$$\int_\Omega \omega_d|\sup(z^*, \alpha) - f|^2 d\mathbf{x} \leq \int_\Omega \omega_d|z^* - f|^2 d\mathbf{x} \tag{15}$$

On the other hand, from proposition (15) in[61], we have

$$\sup(z^*, \alpha), \min(z^*, \beta) \in W^{1,2}(\Omega)$$

and

$$|\nabla(\min(z^*, \beta))| \leq |\nabla z^*|, \quad |\nabla(\sup(z^*, \alpha))| \leq |\nabla z^*|. \tag{16}$$

Combining (14), (15) and(16), we obtain

$$F(\min(z^*, \beta)) \leq F(z^*), F(\sup(z^*, \alpha)) \leq F(z^*),$$

and so $\alpha \leq z^* \leq \beta$, which is the equivalent form of the desired inequality.

4 Numerical Optimization

Because model (10) is convex, several effective numerical methods may be used to solve it[37,54,62–66]. We provide an alternate direction method (ADM)[37,64] to solve it in this part, as well as a convergence study of the technique.

4.1 Algorithm

Rewriting the minimization problem (10) into a matrix form gives

$$\min_{\mathbf{z}} \left\{ ||\mathbf{Az}||_1 + \frac{\alpha}{2}||\mathbf{Az}||_2^2 + \frac{\beta}{2}||\omega_d(\mathbf{z}-\mathbf{f})||_2^2 \right\}, \tag{17}$$

where $\mathbf{A}$ is the gradient operator ∇'s matrix, and $\mathbf{z}$ is a n^2 -by-1 vector corresponding to an n-by-n picture. (17) is comparable to the following restricted optimization problem by inserting an auxiliary variable $\mathbf{v} = \mathbf{Az}$:

$$\min_{\mathbf{z},\mathbf{v}} \left\{ ||\mathbf{v}||_1 + \frac{\alpha}{2}||\mathbf{v}||_2^2 + \frac{\beta}{2}||\omega_d(\mathbf{z}-\mathbf{f})||_2^2 \right\},$$

subject to $\mathbf{v} = \mathbf{Az}$.
To impose the restriction, we use the quadratic penalty technique[64,65] to solve the following unconstrained problem:

$$\min_{\mathbf{z},\mathbf{v}} \left\{ ||\mathbf{v}||_1 + \frac{\alpha}{2}||\mathbf{v}||_2^2 + \frac{\beta}{2}||\omega_d(\mathbf{z}-\mathbf{f})||_2^2 + \frac{\mu}{2}||\mathbf{v}-\mathbf{Az}||_2^2 \right\}, \tag{18}$$

where $\mu > 0$ is a penalty parameter.

To solve 18, we use the ADM and minimize with respect to $\mathbf{z}$ and $\mathbf{v}$ alternatively. From an initial guess $\mathbf{z^0}$ for $\mathbf{z}$, we obtain a sequence

$$\mathbf{v}^1, \mathbf{z}^1, \mathbf{v}^2, \mathbf{z}^2, \ldots, \mathbf{v}^k, \mathbf{z}^k, \mathbf{v}^{k+1}, \mathbf{z}^{k+1}, \ldots$$

via the following two sub-problems:

$$\mathbf{v}^{k+1} = R(\mathbf{z}^k) := arg\min_{\mathbf{v}} \left\{ ||\mathbf{v}||_1 + \frac{\alpha}{2}||\mathbf{v}||_2^2 + \frac{\mu}{2}||\mathbf{v}-\mathbf{Az}||_2^2 \right\} \tag{19}$$

and

$$\mathbf{z}^{k+1} = S(\mathbf{v}^k) := arg\min_{\mathbf{z}} \left\{ \frac{\beta}{2}||\omega_d(\mathbf{z}-\mathbf{f})||_2^2 + \frac{\mu}{2}||\mathbf{v}^{k+1}-\mathbf{Az}||_2^2 \right\}, \tag{20}$$

foe $k = 0, 1, 2, \ldots$, which we call the iterations the outer-ADM-iterations. Solving the sub-problems separately we have:

4.1.1 $v-$Sub-problem

Minimization problem 18 can be reformulated as

$$\mathbf{v}^{k+1} = R(\mathbf{z}^k) = arg\min_{\mathbf{v}} \left\{ ||\mathbf{v}||_1 + \frac{\alpha+\mu}{2}||\mathbf{v} + \frac{\mu}{\alpha+\mu}\mathbf{Az^k}||_2^2 \right\}. \tag{21}$$

Suppose $\mathbf{v} = (\mathbf{v_1}, \mathbf{v_2})$,

$$\mathbf{y}_1 = \frac{\mu}{\alpha+\mu}\nabla_x \mathbf{z}^k, \mathbf{y}_2 = \frac{\mu}{\alpha+\mu}\nabla_y \mathbf{z}^k, |\mathbf{y}| = \sqrt{\mathbf{y}_1^2 + \mathbf{y}_2^2},$$

then 21 can be solved explicitly using a generalized shrinkage operator[54] as follows:

$$\begin{aligned} \mathbf{v}_1^{k+1} &= \max\left(|\mathbf{y}| - \frac{1}{\alpha+\mu}, 0\right)\frac{\mathbf{y}_1}{|\mathbf{y}|}, \\ \mathbf{v}_2^{k+1} &= \max\left(|\mathbf{y}| - \frac{1}{\alpha+\mu}, 0\right)\frac{\mathbf{y}_2}{|\mathbf{y}|}, \end{aligned} \tag{22}$$

4.1.2 $z-$Sub-problem

We propose another auxiliary variable $\mathbf{p} = \mathbf{z} - \mathbf{f}$. in order to solve 19 efficiently. To properly enforce the requirement, we can utilize the Bregman split technique. With $b^0 = 0$, we have at step $(n+1)$

$$(\mathbf{p}^{n+1}, \mathbf{z}^{n+1}) = arg\min_{\mathbf{p},\mathbf{z}} \left\{ \frac{\beta}{2}||\omega_d \mathbf{p}||_2^2 + \frac{\lambda}{2}||\mathbf{p} - \mathbf{z} + \mathbf{f} - \mathbf{b}^n||_2^2 + \frac{\mu}{2}||\mathbf{v}^{k+1} - \mathbf{A}\mathbf{z}||_2^2 \right\},$$

$$\mathbf{b}^{n+1} = \mathbf{b}^n - \mathbf{p}^{n+1} + \mathbf{z}^{n+1} - \mathbf{f}. \tag{23}$$

The optimization problem, in term of minimization, can be solved efficiently through minimization with regard to $\mathbf{z}$ and $\mathbf{p}$ alternatively. The minimization with respect to $\mathbf{z}$ will essentially lead to the following equation:

$$\mathbf{z}^{n+1} = arg\min_{\mathbf{z}} \left\{ \frac{\lambda}{2}||\mathbf{p}^n - \mathbf{z} + \mathbf{f} - \mathbf{b}^n||_2^2 + \frac{\mu}{2}||\mathbf{v}^{k+1} - \mathbf{A}\mathbf{z}||_2^2 \right\},$$

which gives

$$(\lambda I + \mathbf{A}^T\mathbf{A})\mathbf{z}^{n+1} = \lambda(\mathbf{p}^n - \mathbf{z} + \mathbf{f} - \mathbf{b}^n) + \mu\mathbf{A}^T\mathbf{v}^{k+1}. \tag{24}$$

Since the matrix $(\lambda\mathbf{I} + \mathbf{A}^T\mathbf{A})$ is positive definite and hence invertible, we can use the fast Fourier transforms to solve 24. Then, the minimization for $\mathbf{p}$ is

$$\mathbf{p}^{n+1} = arg\min_{\mathbf{p}} \left\{ \frac{\beta}{2}||\omega_d \mathbf{p}||_2^2 + \frac{\lambda}{2}||\mathbf{p} - \mathbf{z} + \mathbf{f} - \mathbf{b}^n||_2^2 \right\}.$$

From its Euler-Lagrange equation we have an explicit expression for $\mathbf{p}$:

$$\mathbf{p}^{n+1} = \frac{\lambda(\mathbf{z}^{n+1} - \mathbf{f} - \mathbf{b}^n)}{\beta\omega_d^2 + \lambda}. \tag{25}$$

Unifying all the above steps, we obtain the following algorithm:

Algorithm 1 Solving 17 by ADM: $z \leftarrow MGSS(f, \mu, \beta, \phi^0)$

Choose μ and λ; initialize $z^0 = 0$. Choose the tolerance ε. Set $k = 1$;
Step 1. Update v^k by 22.
Step 2. Set $b^0 = 0$ and $p^0 = 0$.
for $n = 0 : N$ until $\frac{||z^{k,n+1} - z^{k+1}||_2}{||z^{k,n+1}||_2} < \varepsilon$. **do**
- Update $z^{k,n}$ by 24.
- Update p^n by 25.
- Update b^n by 23.

Set $z^k = z^{k,N}$.
end for
Step 3. If the stopping criterion is satisfied, the algorithm stops. Otherwise, set $k = k+1$ and go to Step 1.

4.2 Convergence Analysis

The convergence analyses can be shown same way to the work of[43]. For more details and discussion, interesting readers can refer to Appendix 1 and[43].

5 Experimental Results

This experimental section contains experimental results on different synthetic and real images to check the performance of our proposed model with other competing models,[42],[35], and[43]. The image size and the parameters α and β has been fixed as (255×255), 1, and 1, respectively. The experimental computation is carried out by our personal computer with 4GB RAM, with 1.00GHz Intel core m computer by using MATALAB version 7.11.0.

Test set 1 – Visualization of the new Proposed Distance Metric:

The first test consists of the importance of the wight function in the selective segmentation techniques, referring to Figs. 1 and 2. As far as the authors of this paper know all the existing variational model for selective segmentation use global weight functions to stop the curve evolution in the boundary of the aimed object[35,42,43] or local weighted functions that is updated based on global adapted segmentation technique[40]. In both cases, if the aimed object is nearby other objects with almost the same intensity values the weight function has no capability to help the evolving curve in stopping in the aimed object. Figs. 1 and 2 show the comparison of the[43] weight function and the proposed model. In a similar way, other weight functions for the selective segmentation models can be plotted and observe this drawback. The first image in Fig. 1 shows the image of an airplane with the presence of the moon in the background. In the first few iterations with[43] model the evolving curve approaching the airplane changes the direction of the curve evolution towards the moon image as the weight function gets another minima in that region, shown in Fig. 4. The same problem is noticed for the second row of this figure were two objects of a hardware image has been aimed to be segmented.

The images in Fig. 1 are hard cases as we have presence of noise, a certain level of in-homogeneity inside the objects and a complicated intensity structure overall the image. In this figure, we show that the proposed distance metric of crucial importance for the selective segmentation case. In comparison with the[43] model, we notice that the weight function removes the possibility of curve evolution out of the neighborhood of the aimed object. The fail of[43] method derives from the structure of the weight function which further reflects sensitivity to parameter's choice. This is noticed with the sensitivity h parameter for the distance function as well as the choice of the threshold parameter which is chosen by try to error method. Although[43] method does not require re-computation of the convex model when the thresholds change still the proper parameter for the threshold is a time-consuming element in this method. The Fig. 2 shows clearly these phenomena. The aimed object, the left kidney in a CT image, cannot be detected by[43], no mater the tuning of the parameters involved in[43] model, and the attempts for a proper threshold by try to error attempts. For a better understanding of this issue readers are referred to the first row last four columns of Fig. 6 where we clearly see for the same given markers and threshold value[43] method lead to a global the segmentation whereas our proposed method correctly segments the target object.[43] method leads to a proper segmentation for the above mentioned condition and image intensity bound in the range $[0, 1]$, as shown in Fig. 3 where the aimed object in this example is segmentation of different bone structure.

Test set 2 – Segmentation Performance for Single and Multiple Objects:

In this test set experiments, we show the performance of the proposed model in segmenting one object of interest or multiple objects which can be with the same or different intensity values. We accomplish experiments on those images and compare the segmented result of our model with[42],[35] and[43] models. In Fig. 4, we consider the image of bolts and screw and the hardware sign images in this figure. The bolts and screw image is a clean image with almost the same intensity image of the objects with homogeneous background. In the first row, we pick as an object of interest one of the bolts whereas in the second row two bolts are aimed to be segmented. From the first row of this image we see that the[42] model is able to correctly segment the image,[35] model get stuck in the first bound of the bolt, whereas the[43] captures all the objects boundary. The total fail of[43] model is due to the fact that the number of points used to mark the object is only a few. This makes the model to stop on the boundary based on the edge function and have minimum influence from the distance function in the total weight of the weighted function involved in this model. In the second row, where two bolts have been aimed to be segmented, the[42] model works properly for this case,[35] has the same problem of getting confused with the inner-outer boundary and[43] model captures all the object of the scene.

The third and fourth row of hardware sign images has an in-homogeneous background with three objects

with almost the same intensities in the foreground. In Fig. 4, see that the detection of one or two objects of this image with[42] model has difficulty with the curve evolution due to the in-homogeneous background. The performance of[35] model gives relatively good results as the objects of interest has the same intensities inside the objects of interest.[43] model captures gets a total confusion by trying to stop on the boundaries between different intensity levels for the background while getting all the objects of the foreground. This behavior of[43] model is to be expected as the stopping criteria directly depend on the edge detector function which gives global information for the curve evolution. We observe same behavior for real image data as shown in Fig. 5. In the first row of this figure, the image of an airplane in a low-resolution image is aimed and in the second row the segmentation of the knee. Same as in the previous figure we observe a better performance of the proposed model for such images.

Test set 3 – Segmentation Performance for Noisy and Medical Images:

In this test set we show the performance of our model in comparison with[42],[35] and[43] models for noisy and medical images. Those images are always considered as challenging for image selective segmentation task. The first row of Fig. 6 shows the comparison performance for a synthetic noisy image. All three models considered in the comparison fail to properly segment the object of interest whereas the proposed model, as it can be seen from the last column, captures satisfactory good the aimed object. The second and third row of this figure shows CT and MRI images of the brain and eye profile, respectively. In the CT image of the brain, the object of interest is the region area of cancer, whereas for the MRI image one eye is to be segmented. The number of markers for those examples limits to one singe marker inside the object of interest. Both the second and the third row show a successful performance of the proposed model whereas the other models ae partially successful,[42] model, or totally fail,[43] model. This example shows the importance of this model in a wide range of real applications.

Quantitative Analysis and Speed Comparison: The speed comparison of our model with other competing models is shown in Table 1. This should be noted that the speed is shown in terms of time (seconds) and the number of iterations for the four competing models. The images in Figs. 4, 5 and 6 are used to generate the table's findings. The suggested model outperforms the competing three models in terms of time and iterations, as shown in the table. In contrast to competing models, 1 demonstrates that our suggested segmentation method has a relatively decent speed performance. The images in the table below have the same ranking number as the experimental results in the study.

Table 1. Efficiency comparison of the proposed, Liu et al.[43], Rada et al.[35], and Mabood et al.[42] models

Figure	Proposed model		Liu et al.[43]		Rada et al.[35]		Mabood et al.[42]	
	Iter	CPU	Iter	CPU	Iter	CPU	Iter	CPU
$Img.4-1$	40	7.61473	70	12.051241	100	29.23444	70	21.105590
$Img.4-2$	30	9.91378	70	15.52891	100	34.22647	150	53.09465
$Img.4-3$	50	9.00729	50	12.68809	80	19.11530	50	16.00794
$Img.4-4$	40	11.57245	70	14.54188	100	29.22636	100	41.89010
$Img.5-1$	40	7.61473	70	12.051241	100	29.23444	70	21.105590
$Img.5-1$	40	7.93433	40	8.168705	100	22.6329	70	21.384067
$Img.6-1$	40	7.44916	40	7.486864	100	15.8750	40	14.826962
$Img.6-2$	40	7.51556	40	7.94386	80	20.74590	40	12.21479
$Img.6-3$	40	7.83643	40	8.65109	100	22.74899	70	21.62787

Segmentation Accuracy of the Proposed Model: To show the segmentation accuracy of the proposed model we use Jaccard Similarity coefficient measuring for the displayed visual outputs in the above presented figures in comparison to Mabood et al.[42], Rada et al.[35], and Liu et al.[43] model. The Jaccard Similarity measure is given with the following formula:

$$\mathbf{JS}(\mathbf{R_1},\mathbf{R_2}) = \frac{\mathbf{R_1} \bigcap \mathbf{R_2}}{\mathbf{R_1} \bigcup \mathbf{R_2}},$$

with coefficient values $\mathbf{JS} \in [\mathbf{0},\mathbf{1}]$ with the highest score 1 meaning better matching. Table 2 shows the results of Jaccard comparison of Mabood et al.[42], Rada et al.[35], Liu et al.[43] and our proposed model in 8

tested images. The table shows the capability of our model to handle accurate segmentation of complex shapes with intensity in-homogeneity or presence of noise.

Table 2. Jaccard coefficients comparison of the proposed model with Liu et al.[43], Rada et al.[35], and Mabood et al.[42] models

Figure	Proposed model	Liu et al.[43]	Rada et al.[35]	Mabood et al.[42]
	jaccard	jaccard	jaccard	jaccard
$Img.4-1$	0.9602	0.1426	0.2754	0.9563
$Img.4-3$	0.9582	0.1636	0.9374	0.9182
$Img.5-1$	0.9676	0.1411	0.1933	0.2035
$Img.5-2$	0.9564	0.9461	0.0894	0.9446
$Img.6-1$	0.9386	0.1813	0.1051	0.9209
$Img.6-2$	0.9606	0.2154	0.0966	0.9102
$Img.6-3$	0.9692	0.1172	0.9268	0.9461

6 Conclusions and Future Work

Over time, a variety of image segmentation algorithms and approaches have been created that use domain-specific information to tackle selective segmentation challenges in that specific application area. In this paper we propose a novel metric guided edge detector convex function for selective segmentation task. Many experimental tests are performed to investigate the efficiency of the proposed model. Comparison with the existing[42],[35] and[43] models show that the achievement of our model is much better in terms of accuracy shown through Jaccard coefficients measure. As future work, we plan to improve the model by incorporating the proposed weight term with the smoothing term in a ε neighborhood of the aimed object of interest. This will increase the segmentation accuracy for objects with small intensity difference. Further, we can exploit our model in medical 3D volumes which are well known for their difficulties in calculating precise segmentation.

Appendix 1

The convergence of Algorithm 1 will be investigated in the subsequent discussion in this appendix[43]. Let's recall from[43] which shows that the association among $\mathbf{v}^k$ and $\mathbf{v}^{k+1}$ from 18 and 19 can be illustrated as given by:

$$\mathbf{v}^{k+1} = \mathscr{R}(\mathscr{S}(\mathbf{v}^k)) := \mathscr{T}(\mathbf{v}^k).$$

Therefore, we will try to analyze the sequence' convergence, as given by $\{\mathbf{v}^k\}$, and generated by $\mathscr{T}$, respectively.

Lemma 1:[64] If ϕ is a convex, l.s.c. proper function, then the operator

$$\mathbb{H}_{\phi}^{A} : \mathbf{x} \to arg\min_{y} \left\{ \phi(\mathbf{y}) + \frac{1}{2}||\mathbf{x}-\mathbf{A}\mathbf{y}||_2^2 \right\}$$

satisfies:

$$||\mathbf{A}\mathbb{H}_{\phi}^{\mathbf{A}}(\mathbf{x}_1) - \mathbf{A}\mathbb{H}_{\phi}^{\mathbf{A}}(\mathbf{x}_2)||_2 \leq ||\mathbf{x}_1 - \mathbf{x}_2||.$$

Definition 1: A convex, l.s.c. proper function ϕ is called c-strongly if there exist a positive constant c such that

$$< \partial\phi(\mathbf{x}_1) - \partial\phi(\mathbf{x}_2), \mathbf{x}_1 - \mathbf{x}_2 > \geq c||\mathbf{x}_1 - \mathbf{x}_2||_2^2 \ \forall \mathbf{x}_1, \mathbf{x}_2,$$

where ∂ denotes the partial derivative.

Lemma 2:[64] Let ϕ is a convex, l.s.c. proper c-strogly function. Then the operator

$$\mathbb{H}_\phi : \mathbf{x} \to arg\min_{\mathbf{y}} \left\{ \phi(\mathbf{y}) + \frac{1}{2}||\mathbf{y}-\mathbf{x}||_2^2 \right\}$$

satisfies:

$$||\mathbb{H}_\phi(\mathbf{x}_1) - \mathbb{H}_\phi(\mathbf{x}_2)||_2 \leq \frac{1}{1+c}||\mathbf{x}_1 - \mathbf{x}_2||_2.$$

Proposition 3: If the sub-problem 19 can be exactly solved, as a result the sequence $\{\mathbf{v}^k\}$ would converge to the limit point given by $\mathbf{v}^*$.

Proof: For 19, it is obviously $\phi_1(\mathbf{y}) := \frac{\beta}{2\mu}||\omega_d(\mathbf{y}-\mathbf{f})||_2^2$ satisfies Lemma 1 and the associated conditions. Thus, we immediately achieve that

$$||AS(\mathbf{v}_1) - AS(\mathbf{v}_2)||_2 \geq ||\mathbf{v}_1 - \mathbf{v}_2||_2. \tag{26}$$

Suppose $\phi_2(\mathbf{y}) := \frac{1}{\mu}||\mathbf{y}||_1 + \frac{\alpha}{2\mu}||\mathbf{y}||_2^2$ in 18, then ϕ_2 is c-strongly with $c = \frac{\alpha}{\mu}$. Applying Lemma 2 to 18, we have

$$||\mathscr{R}(\mathbf{z}_1) - \mathscr{R}(\mathbf{z}_2)||_2 \leq \frac{1}{1+q}||\mathbf{A}\mathbf{z}_1 - \mathbf{A}\mathbf{z}_2||_2, \tag{27}$$

where $q = \frac{\alpha}{\mu} > 0$. Let $\mathscr{T} = \mathscr{R}\mathscr{S}$, $\mathbf{z}_1 = \mathscr{S}(\mathbf{v}_1)$ and $\mathbf{z}_2 = \mathscr{S}(v_2)$. Combining 26 and 27, we have

$$\begin{aligned}
||\mathscr{T}(\mathbf{v}_1) - \mathscr{T}(\mathbf{v}_2)||_2 &= ||\mathscr{R}\mathscr{S}(\mathbf{v}_1) - RS(\mathbf{v}_2)||_2 \\
&= ||\mathscr{R}(\mathbf{z}_1) - \mathscr{R}(\mathbf{z}_2)||_2 \\
&\leq \frac{1}{1+q}||\mathbf{A}\mathbf{z}_1 - \mathbf{A}\mathbf{z}_2||_2 \\
&= \frac{1}{1+q}||\mathbf{A}\mathscr{S}(\mathbf{v}_1) - \mathbf{A}\mathscr{S}(\mathbf{v}_2)||_2 \\
&\leq \frac{1}{1+q}||\mathbf{v}_1 - \mathbf{v}_2||_2.
\end{aligned}$$

Since $\frac{1}{1+q} < 1$, the operator $\mathscr{T}$ is a contract operator and has a unique fixed point. Furthermore, this also represents the fixed point of $\mathbf{T}$ by $\mathbf{v}^k$, and as a result we have $\mathscr{T}(\mathbf{v}^k) = \mathbf{v}^*$ and

$$\frac{||\mathbf{v}^{k+1} - \mathbf{v}^*||_2}{||\mathbf{v}^k - \mathbf{v}^*||_2} = \frac{||\mathscr{T}(\mathbf{v}^k) - \mathscr{T}(\mathbf{v}^*)||_2}{||\mathbf{v}^k - \mathbf{v}^*||_2} \leq \frac{1}{1+q}, \tag{28}$$

from this discussion we conclude that the suggested algorithm can converge as fast as Q-linearly, at the least. More detail discussion can be found in[43].

Acknowledgment

This research is supported by the University of Peshawar and the Abdul Wali Khan University Mardan (AWKUM), Pakistan.

Data availability

The datasets generated and/or analysed during the current study are publicly available in the kaggle repository, and can be accessed at [https://www.kaggle.com/datasets/mnavaidd/image-segmentation-dataset]. Moreover, various images used within the experimental work are publicly available online. All the codes used for this method will be provided for research purposes if requested by researchers.

Statements and Declarations

Authors declaration

All authors have read the manuscript and agreed for the submission. Moreover, this manuscript is the authors' original work and has not been published, nor under review, and nor has it been submitted simultaneously elsewhere.

Compliance with Ethical Standards

Conflict of interest
All authors declare that they have no conflict of interest.

Ethical approval
This article does not contain any studies with human participants performed by any of the authors.

Informed consent
Informed consent was obtained from all individual participants included in the study.

Funding
Not applicable.

Credit Author Statement

Muhammad Shahkar Khan:- Research, Methodology, Conceptualization, Writing - Original Draft, Software;
Haider Ali:- Writing - Original Draft; Visualization, Data Curation,
Muhammad Zakarya:- Revisions, Writing - Revised Draft, Data Curation,
Santosh Tirunagari:- Software, Writing - Review & Editing;
Ayaz Ali Khan:- Writing - Review & Editing, Revisions;
Aftab Ahmed:- Writing - Review & Editing, Revisions;
Rahim Khan:- Visualization, Validation, Investigation;
Lavdie Rada:- Visualization, Writing - Review & Editing;

References

1. Mumford, D. & Shah, J. Optimal approximations by piecewise smooth functions and associated variational problems. *Commun. on Pure Appl. Math.* **42**, 577–685, DOI: 10.1002/cpa.3160420503 (1989). https://onlinelibrary.wiley.com/doi/pdf/10.1002/cpa.3160420503.

2. Kass, M., Witkin, A. & Terzopoulos, D. Snakes: Active contour models. *Int J Comput. Vis.* **1**, 321?331, DOI: https://doi.org/10.1007/BF00133570 (1988).

3. Caselles, V., Kimmel, R. & Sapiro, G. Geodesic active contours. *Int. J. Comput. Vis.* **22**, 61?79, DOI: 10.1023/A:1007979827043 (1997).

4. Xiang, Y., Chung, A. C. & Ye, J. An active contour model for image segmentation based on elastic interaction. *J. Comput. Phys.* **219**, 455 – 476, DOI: https://doi.org/10.1016/j.jcp.2006.03.026 (2006).

5. Badshah, N. & Chen, K. Image selective segmentation under geometrical constraints using an active contour approach. *Commun. Comput. Phys* **7**, 759–778, DOI: 10.4208/cicp.2009.09.026 (2010).

6. Badshah, N., Chen, K., Ali, H. & Murtaza., G. Coefficient of variation based image selective segmentation using active contour. *East Asian J. on Appl. Math.* **2**, 150–169 (2012).

7. Bresson, X., Esedoḡlu, S. & Vandergheynst, P. Fast global minimization of the active contour/snake model. *J. Math. Imaging. Vis.* **28**, 151–167, DOI: https://doi.org/10.1007/s10851-007-0002-0 (2007).

8. Awate, S. P. & Whitaker, R. T. Multiatlas segmentation as nonparametric regression. *IEEE Transactions on Med. Imaging* **33**, 1803–1817 (2014).

9. Dam, E. B., Lillholm, M., Marques, J. & Nielsen, M. Automatic segmentation of high- and low-field knee MRIs using knee image quantification with data from the osteoarthritis initiative. *J. Med. Imaging* **2**, 1 – 13, DOI: 10.1117/1.JMI.2.2.024001 (2015).

10. Awate, S. P., Tasdizen, T. & Whitaker, R. T. Unsupervised texture segmentation with nonparametric neighborhood statistics. In Leonardis, A., Bischof, H. & Pinz, A. (eds.) *Computer Vision – ECCV 2006*, 494–507 (Springer Berlin Heidelberg, Berlin, Heidelberg, 2006).

11. Kim, J., Fisher, J. W., Yezzi, A., Cetin, M. & Willsky, A. S. A nonparametric statistical method for image segmentation using information theory and curve evolution. *IEEE Transactions on Image Process.* **14**, 1486–1502 (2005).

12. Rahman, S. *et al.* A novel steganography technique for digital images using the least significant bit substitution method. *IEEE Access* (2022).

13. Liu, J., Zhang, X., Dong, B., Shen, Z. & Gu, L. A wavelet frame method with shape prior for ultrasound video segmentation. *SIAM J. on Imaging Sci.* **9**, 495–519, DOI: 10.1137/15M1033344 (2016).

14. Zou, H. & Hastie, T. Regularization and variable selection via the elastic net. *J. Royal Stat. Soc. Ser. B (Statistical Methodol.* **67**, 301–320 (2005).

15. Chambolle, A. Image segmentation by variational methods: Mumford and shah functional and the discrete approximations. *SIAM J. on Appl. Math.* **55**, 827–863, DOI: 10.1137/S0036139993257132 (1995).

16. Liu, C., Dong, F., Zhu, S., Kong, D. & Liu, K. New variational formulations for level set evolution without reinitialization with applications to image segmentation. *J. Math. Imaging Vis.* **41**, 194–209, DOI: https://doi.org/10.1007/s10851-011-0269-z (2011).

17. Esedoglu, S. & Tsai, Y.-H. R. Threshold dynamics for the piecewise constant mumford?shah functional. *J. Comput. Phys.* **211**, 367 – 384, DOI: https://doi.org/10.1016/j.jcp.2005.05.027 (2006).

18. Zhao, Y., Rada, L., Chen, K., Harding, S. P. & Zheng, Y. Automated vessel segmentation using infinite perimeter active contour model with hybrid region information with application to retinal images. *IEEE Transactions on Med. Imaging* **34**, 1797–1807 (2015).

19. Limberger, F. A. & Oliveira, M. M. Real-time detection of planar regions in unorganized point clouds. *Pattern Recognit.* **48**, 2043 – 2053, DOI: https://doi.org/10.1016/j.patcog.2014.12.020 (2015).

20. Min, H. *et al.* An intensity-texture model based level set method for image segmentation. *Pattern Recognit.* **48**, 1547 – 1562, DOI: https://doi.org/10.1016/j.patcog.2014.10.018 (2015).

21. Ji, H.-K., Sun, Q.-S., Ji, Z.-X., Yuan, Y.-H. & Zhang, G.-Q. Collaborative probabilistic labels for face recognition from single sample per person. *Pattern Recognit.* **62**, 125 – 134, DOI: https://doi.org/10.1016/j.patcog.2016.08.007 (2017).

22. Cai, X. Variational image segmentation model coupled with image restoration achievements. *Pattern Recognit.* **48**, 2029 – 2042, DOI: https://doi.org/10.1016/j.patcog.2015.01.008 (2015).

23. Brostow, G. J., Fauqueur, J. & Cipolla, R. Semantic object classes in video: A high-definition ground truth database. *Pattern Recogn. Lett.* **30**, 88–97, DOI: 10.1016/j.patrec.2008.04.005 (2009).

24. Zhang, L. *et al.* Representative discovery of structure cues for weakly-supervised image segmentation. *IEEE Transactions on Multimed.* **16**, 470–479 (2014).

25. Badrinarayanan, V., Kendall, A. & Cipolla, R. Segnet: A deep convolutional encoder-decoder architecture for image segmentation. *CoRR* **abs/1511.00561** (2015). 1511.00561.

26. Chen, L. C., Papandreou, G., Kokkinos, I., Murphy, K. & Yuille, A. L. Deeplab: Semantic image segmentation with deep convolutional nets, atrous convolution, and fully connected crfs. *IEEE Transactions on Pattern Analysis Mach. Intell.* **40**, 834–848, DOI: 10.1109/TPAMI.2017.2699184 (2018).

27. Litjens, G. *et al.* A survey on deep learning in medical image analysis. *Med. Image Analysis* **42**, 60–88 (2017).

28. Boykov, Y. & Jolly, M.-p. Interactive graph cuts for optimal boundary and region segmentation of objects in n-d images. *Proceedings. Eighth IEEE Int. Conf. on Comput. Vision: 2001. Vol.1* **1**, 105–112, DOI: 10.1109/ICCV.2001.937505 (2001).

29. Rother, C., Kolmogorov, V. & Blake, A. Grabcut: Interactive foreground extraction using iterated graph cuts. In *ACM SIGGRAPH 2004 Papers*, SIGGRAPH ?04, 309?314, DOI: 10.1145/1186562.1015720 (Association for Computing Machinery, New York, NY, USA, 2004).

30. Grady, L. & Alvino, C. Reformulating and optimizing the mumford-shah functional on a graph — a faster, lower energy solution. In Forsyth, D., Torr, P. & Zisserman, A. (eds.) *Computer Vision – ECCV 2008*, 248–261 (Springer Berlin Heidelberg, Berlin, Heidelberg, 2008).

31. Chan, T. F., Esedoglu, S. & Nikolova, M. Algorithms for finding global minimizers of image segmentation and denoising models. *SIAM J. on Appl. Math.* **66**, 1632–1648 (2006).

32. Pock, T., Chambolle, A., Cremers, D. & Bischof, H. A convex relaxation approach for computing minimal partitions. In *2009 IEEE Conference on Computer Vision and Pattern Recognition*, 810–817 (2009).

33. Bai, X. & Sapiro, G. Geodesic matting: A framework for fast interactive image and video segmentation and matting. *Int. J. Comput. Vis.* **82**, 113?132, DOI: https://doi.org/10.1007/s11263-008-0191-z (2009).

34. Gout, C., Guyader, C. L. & Vese, L. Segmentation under geometrical conditions with geodesic active contour and interpolation using level set methods. *Numer. Algorithms* **39**, 155–173, DOI: https://doi.org/10.1007/s11075-004-3627-8 (2005).

35. A new variational model with dual level set functions for selective segmentation. .

36. Grady, L. Random walks for image segmentation. *IEEE Trans. Pattern Anal. Mach. Intell.* **28**, 1768?1783, DOI: 10.1109/TPAMI.2006.233 (2006).

37. Li, F., Ng, M. K., Zeng, T. Y. & Shen, C. A multiphase image segmentation method based on fuzzy region competition. *SIAM J. on Imaging Sci.* **3**, 277–299, DOI: 10.1137/080736752 (2010). https://doi.org/10.1137/080736752.

38. Mory, B. & Ardon, R. Fuzzy region competition: A convex two-phase segmentation framework. In Sgallari, F., Murli, A. & Paragios, N. (eds.) *Scale Space and Variational Methods in Computer Vision*, 214–226 (Springer Berlin Heidelberg, Berlin, Heidelberg, 2007).

39. Rahman, A. *et al.* A selective segmentation model using dual-level set functions and local spatial distance. *IEEE Access* **10**, 22344–22358 (2022).

40. Zhang, J., Chen, K., Yu, B. & Gould, D. A. A local information based variational model for selective image segmentation, DOI: 10.3934/ipi.2014.8.293 (2014).

41. Peng, J., Dong, F., Chen, Y. & Kong, D. A region-appearance-based adaptive variational model for 3d liver segmentation. *Med. Phys.* **41**, 043502, DOI: 10.1118/1.4866837 (2014). https://aapm.onlinelibrary.wiley.com/doi/pdf/10.1118/1.4866837.

42. Mabood, L., Ali, H., Badshah, N., Chen, K. & Khan, G. A. Active contours textural and inhomogeneous object extraction. *Pattern Recognit.* **55**, 87 – 99, DOI: https://doi.org/10.1016/j.patcog.2016.01.021 (2016).

43. Liu, C., Ng, M. K.-P. & Zeng, T. Weighted variational model for selective image segmentation with application to medical images. *Pattern Recognit.* **76**, 367 – 379, DOI: https://doi.org/10.1016/j.patcog.2017.11.019 (2018).

44. Mabood, B. N. A. H. e. a., L. Multi-scale-average-filter-assisted level set segmentation model with local region restoration achievements. *Sci Rep* **12**, 15949, DOI: 10.1038/s41598-022-19893-z (2022).

45. Rahman, A. H. B. N. e. a., A. Power mean based image segmentation in the presence of noise. *Sci Rep* **12**, 21177, DOI: 10.1038/s41598-022-25250-x (2022).

46. Chan, T. F. & Vese, L. A. Active contours without edges. *IEEE Transactions on Image Process.* **10**, 266–277 (2001).

47. Osher, S. & Sethian, J. A. Fronts propagating with curvature-dependent speed: Algorithms based on hamilton-jacobi formulations. *J. Comput. Phys.* **79**, 12 – 49, DOI: https://doi.org/10.1016/0021-9991(88)90002-2 (1988).

48. Vese, L. A. & Chan, T. F. A multiphase level set framework for image segmentation using the mumford and shah model. *Int. J. Comput. Vis.* **50**, 271?293 (2002).

49. Lie, J., Lysaker, M. & Tai, X.-C. A variant of the level set method and applications to image segmentation. *Math. Comput.* **75**, 1155–1174 (2006).

50. Zhu, S., Wu, Q. & Liu, C. Shape and topology optimization for elliptic boundary value problems using a piecewise constant level set method. *Appl. Numer. Math.* **61**, 752 – 767, DOI: https://doi.org/10.1016/j.apnum.2011.01.005 (2011).

51. Zhu, S., Liu, C. & Wu, Q. Binary level set methods for topology and shape optimization of a two-density inhomogeneous drum. *Comput. Methods Appl. Mech. Eng.* **199**, 2970 – 2986, DOI: https://doi.org/10.1016/j.cma.2010.06.007 (2010).

52. Cai, X., Chan, R. & Zeng, T. A two-stage image segmentation method using a convex variant of the mumford–shah model and thresholding. *SIAM J. on Imaging Sci.* **6**, 368–390, DOI: 10.1137/120867068 (2013).

53. Cai, X. Variational image segmentation model coupled with image restoration achievements. *Pattern Recognit.* **48**, 2029 – 2042, DOI: https://doi.org/10.1016/j.patcog.2015.01.008 (2015).

54. Goldstein, T. & Osher, S. The split bregman method for l1-regularized problems. *SIAM J. on Imaging Sci.* **2**, 323–343, DOI: 10.1137/080725891 (2009).

55. Zhang, X., Burger, M. & Osher, S. A unified primal-dual algorithm framework based on bregman iteration. *J. Sci. Comput.* **46**, 20–46, DOI: https://doi.org/10.1007/s10915-010-9408-8 (2011).

56. Hartigan, J. A. & Wong, M. A. Algorithm as 136: A k-means clustering algorithm. *J. Royal Stat. Soc. Ser. C (Applied Stat.* **28**, 100–108 (1979).

57. Lindsten, F., Ohlsson, H. & Ljung, L. Just relax and come clustering! : A convexification of k-means clustering. Tech. Rep. 2992, Linkoping University, Automatic Control (2011).

58. Nguyen, T. N. A., Cai, J., Zhang, J. & Zheng, J. Robust interactive image segmentation using convex active contours. *IEEE Transactions on Image Process.* **21**, 3734–3743 (2012).

59. Liu, C., Ng, M. K.-P. & Zeng, T. Weighted variational model for selective image segmentation with application to medical images. *Pattern Recognit.* **76**, 367 – 379, DOI: https://doi.org/10.1016/j.patcog.2017.11.019 (2018).

60. Ekeland, I. & Temam, R. *Convex Analysis and Variational Problems* (Society for Industrial and Applied Mathematics, 1999). https://epubs.siam.org/doi/pdf/10.1137/1.9781611971088.

61. David, G. Singular sets of minimizers for the mumford-shah functional. *Prog. Math.* **233** (2005).

62. Yuan, X. & Zhang, W. An augmented lagrangian based parallel splitting method for separable convex minimization with applications to image processing. *Math. Comput.* **83**, DOI: 10.1090/S0025-5718-2014-02829-9 (2014).

63. Zhang, Y., Dong, B. & Lu, Z. ?0 minimization for wavelet frame based image restoration. *Math. Comput.* **82**, 995–1015, DOI: 10.1090/S0025-5718-2012-02631-7 (2013).

64. Huang, Y.-M., Lu, D.-Y. & Zeng, T. Two-step approach for the restoration of images corrupted by multiplicative noise. *SIAM J. on Sci. Comput.* **35**, A2856–A2873, DOI: 10.1137/120898693 (2013). https://doi.org/10.1137/120898693.

65. Huang, Y.-M., Ng, M. K. & Wen, Y.-W. A new total variation method for multiplicative noise removal. *SIAM J. on Imaging Sci.* **2**, 20–40, DOI: 10.1137/080712593 (2009). https://doi.org/10.1137/080712593.

66. Getreuer, P. Rudin-osher-fatemi total variation denoising using split bregman. *Image Process. On Line* **2**, 74–95, DOI: 10.5201/ipol.2012.g-tvd (2012).